Engineering Transactions, **73**(1): 75–87, 2025, https://doi.org/10.24423/engtrans.3472.2025
Institute of Fundamental Technological Research Polish Academy of Sciences (IPPT PAN)
Université de Lorraine • Poznan University of Technology

Technical Note

Vibrations of a Rotating Hanged String with a Heavy Tip Mass

Mehmet Pakdemirli

Mechanical Engineering Department, Manisa Celal Bayar University
Yunusemre, Manisa, Turkey; e-mail: pakdemirli@gmail.com

The vibrations of a string-mass system are considered. A heavy mass is suspended from a string, and the system is subjected to axial rotation. The partial differential equation modeling the system's dynamics is first derived. For uniform axial rotation, exact analytical solutions are given. For harmonically fluctuating rotation speeds, an approximate solution is found using the method of multiple scales to analyze the system's principal parametric resonances. The stability of the system is examined both analytically and numerically. The analytically derived stability boundaries qualitatively match the behavior observed in numerical simulations. With some transformations, the system can also be reduced to a standard Mathieu equation.

Keywords: string-mass; perturbation; rotation; principal parametric resonances; stability; Mathieu equation.

1. Introduction

The vibrations of hanging strings have attracted the attention of many researchers. Chains, strips, ropes and strings with negligible bending stiffness all belong to the same class. The lower end of the string may be free or constrained by an end condition or a tip mass, while the upper end may be fixed or subjected to vibrations in lateral or vertical directions. If the lower end of the string is free, the system's dynamics can become extremely complex. A fundamental study based on the dynamic equilibrium of an eccentrically rotating hanging rope was conducted, in which the shape functions of the rope were analytically calculated [1]. In that study, the rope was confined to a two-dimensional rotating space. It is noted that linear oscillations of freely hanging ropes introduce a paradox if the lower end is not free, and this paradox can be resolved by introducing slight bending stiffness [2]. Three-dimensional analysis of strings can display more complex whirling-type motions. Both theoretical and experimental

studies were reported on such behavior in [3]. Whirling modes of idealized inextensible strings were also discussed in [4]. Additionally, vertical shaking applied to a hanging chain has shown to induce complex dynamics leading to chaotic motion [5]. Bifurcation diagrams and equilibrium shapes of strings were also depicted [6].

Adding a heavy tip mass enhances the stability of the system. In a simplified crane model, the vibrations of tethered mass-spring systems were considered [7]. A generalized approach was proposed, including the rotational moment of inertia of the tip mass while neglecting the axial rotation of the cord [8]. The critical rotation speeds of a hanging chain-mass system, which result in nontrivial solutions were determined [9]. Additionally, the vibrations of a heavy string-mass system were investigated when the top end was subjected to lateral excitations [10]. Rather than employing a continuum model based on differential equations, a discrete analysis using difference equations was performed to describe the dynamics of axially rotating chain-mass systems [11]. Furthermore, for a system with both ends pinned and undergoing uniform axial rotation, the resonances of heavy elastic cables were investigated [12].

In all the previous studies cited, the string is either stationary or undergoing uniform axial rotation. In this study, in addition to analyzing the uniform axial rotation of a string-mass system, variable rotation case is also considered. Specifically, a harmonically varying angular speed about a mean speed is assumed in the analysis. After deriving the mathematical model, exact analytical solutions are given for uniform rotation speeds. For variable speeds, an approximate analytical solution is obtained using the method of multiple scales to analyze principal parametric resonances. For applications of this method to a wide range of mathematical physics problems, see [13] and [14]. The stability boundaries separating stable and unstable regions are calculated analytically. Numerical simulations confirm the qualitative behavior of the approximate analytical solutions. It is shown that the system can be reduced to a standard Mathieu equation via a special time transformation, allowing the use of standard stability charts for the Mathieu equation. Since the axial rotations are centric, the problem reduces to an eigenvalue-eigenfunction problem, where eigenvalues represent natural frequencies and eigenfunctions correspond to vibration mode shapes. However, if rotation is eccentric, the problem is no longer an eigenvalue-eigenfunction problem, as this structure breakdown, allowing nontrivial solutions at all rotation speeds. For a similar analysis of rotational motion in beams and relevant discussions, see [15]. In a closely related study of hanging beams, vibrations under variable rotation speeds were also analyzed, see [16]. Additionally, drilling machines with a heavy tip mass and negligible flexural rigidity due to high slenderness ratios may exhibit similar behavior, although a precise analysis for such systems must account for flexural rigidity.

2. Mathematical model

A string of length l and mass/length ρ is suspended from the top, with a heavy tip mass M attached at the lower end, rotating at an angular speed Ω, as shown in Fig. 1.

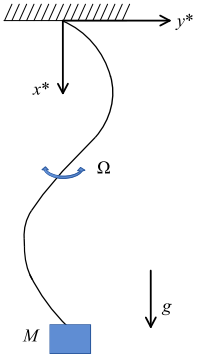

Fig. 1. Sketch of the problem.

To derive the equation of motion, the following assumptions are made: (1) The vibrations are confined to a two-dimensional space rotating with the same angular speed as the system. (2) The total mass of the string is small compared to the tip mass, i.e., $\rho\ell \ll M$. (3) The tip mass is heavy and perfectly symmetric, remaining on the rotation axis without any lateral displacement. The free-body diagram of a small portion of the string with mass $\mathrm{d}m = \rho\,\mathrm{d}x^*$ is given in Fig. 2.

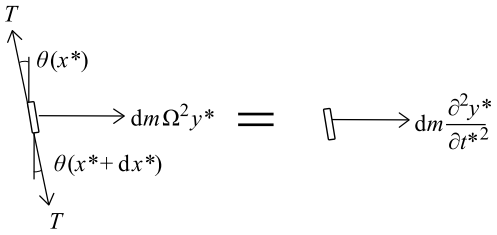

Fig. 2. Free-body diagram of a differential element.

In accordance with the second assumption, the tension force can be assumed constant and approximately equal to the weight of the tip mass. The equation of motion in the lateral direction is:

$$-T\sin\left(\theta(x^*)\right) + T\sin\left(\theta(x^* + \mathrm{d}x^*)\right) + \mathrm{d}m\Omega^2 y^* = \mathrm{d}m\frac{\partial^2 y^*}{\partial t^{*2}}, \tag{2.1}$$

where $\mathrm{d}m = \rho\,\mathrm{d}x^*$. Expanding the sine function in a Taylor series:

$$\sin\left(\theta(x^* + \mathrm{d}x^*)\right) \cong \sin\left(\theta(x^*)\right) + \cos\left(\theta(x^*)\right)\frac{\partial\theta}{\partial x^*}\,\mathrm{d}x^*. \tag{2.2}$$

Substituting this into Eq. (2.1) and assuming $\cos(\theta(x^*)) \cong 1$ for small angles, we obtain, after simplification:

$$T\frac{\partial\theta}{\partial x^*} + \rho\,\Omega^2 y^* = \rho\frac{\partial^2 y^*}{\partial t^{*2}}. \tag{2.3}$$

Since $\tan\theta \cong \theta = \frac{\partial y^*}{\partial x^*}$ and for $T = Mg$, the equation of motion simplifies to:

$$Mg\frac{\partial^2 y^*}{\partial x^{*2}} + \rho\,\Omega^2 y^* = \rho\frac{\partial^2 y^*}{\partial t^{*2}}. \tag{2.4}$$

One set of initial and boundary conditions for the problem may be defined as follows:

$$y^*(0,t^*) = 0, \quad y^*(\ell,t^*) = 0, \quad y^*(x^*,0) = f(x^*), \quad \frac{\partial y^*}{\partial t^*}(x^*,0) = 0, \tag{2.5}$$

where the function $f(x^*)$ satisfies the condition $f(0) = f(\ell) = 0$. Equation (2.4) has the same structure as a mathematical model describing the transverse vibrations of a string exhibiting negative stiffness. If, instead of the weight Mg, the tension T is used, and instead of the term $\rho\,\Omega^2$, the stiffness k is introduced the equation takes the form of a system with negative stiffness. Negative stiffness will definitely destabilize the motion, a phenomenon that also occurs in our system, as will be demonstrated in the subsequent analysis.

It is better to express the equations in a non-dimensional form for compactness and reduction of the physical parameters involved in the model. The dimensionless spatial coordinates and time are defined to be

$$x = \frac{x^*}{\ell}, \qquad y = \frac{y^*}{\ell}, \qquad t = \frac{t^*}{T}. \tag{2.6}$$

Inserting them into Eqs. (2.4) and (2.5), choosing

$$T = \sqrt{\frac{\rho}{Mg}}\ell \tag{2.7}$$

the dimensionless system is

$$\frac{\partial^2 y}{\partial x^2} + a^2 y = \frac{\partial^2 y}{\partial t^2}, \tag{2.8}$$

$$y(0,t) = 0, \qquad y(1,t) = 0, \qquad y(x,0) = f(x), \qquad \frac{\partial y}{\partial t}(x,0) = 0, \tag{2.9}$$

where

$$a^2 = \frac{\rho\,\Omega^2\ell^2}{Mg} \tag{2.10}$$

is the ratio of the centripetal force exerted to the string to the gravity force of the tip mass.

3. Constant rotation speed

An exact analytical solution is available for the case of constant rotation speed. Assume a solution of the form:

$$y(x,t) = \sum_{n=1}^{\infty} u_n(t) \sin(n\pi x). \tag{3.1}$$

Alternatively, the complex exponential method outlined in [17] can also be used. The solution satisfies the first two boundary conditions. Substituting Eq. (3.1) into Eq. (2.8), the equation for the generalized coordinates is obtained as:

$$\ddot{u}_n + (n^2\pi^2 - a^2)u_n = 0. \tag{3.2}$$

Defining the natural frequencies as:

$$\omega_n^2 = n^2\pi^2 - a^2, \tag{3.3}$$

the solution to the problem

$$\ddot{u}_n + \omega_n^2 u_n = 0 \tag{3.4}$$

is given by:

$$u_n = c_{1n}\cos(\omega_n t) + c_{2n}\sin(\omega_n t). \tag{3.5}$$

The last condition in Eq. (2.9) requires $\dot{u}_n(0) = 0$ or $c_{2n} = 0$. The remaining non-homogenous condition requires:

$$f(x) = \sum_{n=1}^{\infty} c_{1n}\sin(n\pi x), \tag{3.6}$$

and the Fourier coefficients for the problem are solved from above as:

$$c_{1n} = 2\int_0^1 f(x)\sin(n\pi x)\,\mathrm{d}x. \tag{3.7}$$

The general solution is then:

$$y(x,t) = \sum_{n=1}^{\infty} 2\left(\int_0^1 f(x)\sin(n\pi x)\,\mathrm{d}x\right)\cos\left(\sqrt{n^2\pi^2 - a^2}\,t\right)\sin(n\pi x). \tag{3.8}$$

As the rotation speed increases, the natural frequencies decrease due to an increase in the dimensionless parameter a. The first three natural frequencies are shown in Fig. 3.

When the rotation speed reaches a critical value, the natural frequency for a particular mode of vibration becomes zero, leading to a phenomenon known as divergence instability.

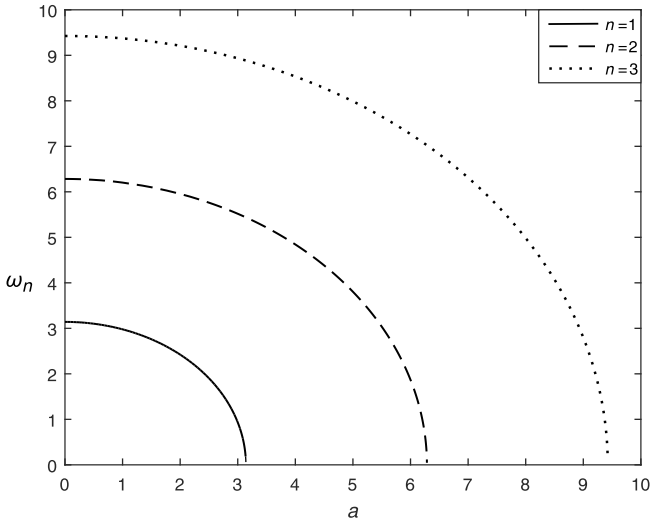

FIG. 3. Natural frequencies of the system.

4. Variable rotation speed

In this section, a harmonically varying rotation speed about a mean speed is considered:

$$\Omega^2 = \Omega_0^2 + \varepsilon\,\Omega_1^2 \sin\left(w^* t^*\right), \tag{4.1}$$

where Ω_0 is the mean speed of rotation, $\varepsilon \ll 1$ is inserted to ensure that the speed fluctuation amplitudes $\varepsilon\,\Omega_1$ are small, and w^* is the dimensional fluctuation frequencies. The parameter a given in Eq. (2.10) is no longer constant, but varies as follows:

$$a^2 = a_0^2 + \varepsilon a_1^2 \sin\left(wt\right), \tag{4.2}$$

where

$$a_0^2 = \frac{\rho\,\Omega_0^2 \ell^2}{Mg}, \qquad a_1^2 = \frac{\rho\,\Omega_1^2 \ell^2}{Mg}. \tag{4.3}$$

The dimensionless fluctuation frequency is related to the dimensional frequency by:

$$w = w^* \sqrt{\frac{\rho}{Mg}}\,\ell. \tag{4.4}$$

Substituting Eq. (4.2) into Eq. (2.8), the dynamics of motion are governed by:

$$\frac{\partial^2 y}{\partial x^2} + \left(a_0^2 + \varepsilon a_1^2 \sin\left(wt\right)\right) y = \frac{\partial^2 y}{\partial t^2}. \tag{4.5}$$

Assuming the solution form from Eq. (3.1) again, substituting this solution into Eq. (4.5), the equations for the generalized coordinates are:

$$\ddot{u}_n + \omega_n^2 u_n = \varepsilon a_1^2 \sin(wt)\, u_n, \tag{4.6}$$

where

$$\omega_n = \sqrt{n^2\pi^2 - a^2} \tag{4.7}$$

are the natural frequencies from Eq. (3.3). The initial conditions for the problem reduce to:

$$u_n(0) = 2\int_0^1 f(x)\sin(n\pi x)\,\mathrm{d}x, \qquad \dot{u}_n(0) = 0. \tag{4.8}$$

4.1. Analytical solutions

Principal parametric resonances are the strongest resonance type in such parametrically excited systems. The fluctuation frequency is close to twice the natural frequency of the system, i.e.,

$$w = 2\omega_n + \varepsilon\sigma, \tag{4.9}$$

where σ is the detuning parameter adjusting the proximity of the fluctuation frequency to twice the natural frequency. A perturbative solution using the method of multiple scales [13, 14] will be used to search for approximate analytical solutions. A single perturbation parameter is used in the analysis. For the advantages of using a single parameter instead of multiple parameters, see the detailed calculations given in [18].

An approximate solution of Eq. (4.6) subject to Eq. (4.9) is sought in the form:

$$u_n(t;\varepsilon) = u_{n0}(T_0, T_1) + \varepsilon u_{n1}(T_0, T_1) + ..., \tag{4.10}$$

where $T_0 = t$ and $T_1 = \varepsilon t$ are the fast and slow time scales. The time derivatives are:

$$\frac{\partial}{\partial t} = D_0 + \varepsilon D_1 + ..., \qquad \frac{\partial^2}{\partial t^2} = D_0^2 + 2\varepsilon D_0 D_1 + ..., \tag{4.11}$$

where $D_0 = \frac{\partial}{\partial T_0}$ and $D_1 = \frac{\partial}{\partial T_1}$. The equations are separated at each order:

$$D_0^2 u_{n0} + \omega_n^2 u_{n0} = 0, \tag{4.12}$$

$$D_0^2 u_{n1} + \omega_n^2 u_{n1} = -2D_0 D_1 u_{n0} + a_1^2 \sin(wT_0)\, u_{n0}. \tag{4.13}$$

Solving Eq. (4.12):

$$u_{n0} = B_n(T_1)e^{i\omega_n T_0} + cc = b_n(T_1)\cos\left(\omega_n T_0 + \beta_n(T_1)\right), \tag{4.14}$$

where cc stands for the complex conjugates, B_n represents the complex amplitudes, and b_n and β_n are the real amplitudes and phases, which are related to each other via the polar form:

$$B_n(T_1) = \frac{1}{2}b_n(T_1)e^{i\beta_n(T_1)}. \tag{4.15}$$

Inserting Eqs. (4.14) and (4.9) into Eq. (4.13) and eliminating the secularities yields:

$$-2i\omega_n D_1 B_n + \frac{a_1^2}{2i}\overline{B}_n e^{i\sigma T_1} = 0. \tag{4.16}$$

Substituting the polar form into this equation, and separating the real and imaginary parts, we obtain:

$$\omega_n D_1 b_n + \frac{a_1^2}{4}b_n\cos(\gamma_n) = 0, \tag{4.17}$$

$$\left(\omega_n(D_1\gamma_n - \sigma) - \frac{a_1^2}{2}\sin(\gamma_n)\right)b_n = 0, \tag{4.18}$$

where

$$\gamma_n = \sigma T_1 - 2\beta_n. \tag{4.19}$$

The above equations admit the trivial solution $b_n = 0$. For nontrivial solutions, the amplitude and phase variations are governed by:

$$D_1 b_n = -\frac{a_1^2}{4\omega_n}b_n\cos(\gamma_n), \tag{4.20}$$

$$D_1\gamma_n = \sigma + \frac{a_1^2}{2\omega_n}\sin(\gamma_n). \tag{4.21}$$

The approximate analytical solution is written using Eqs. (3.1), (4.9), (4.10), (4.14), (4.15), and (4.19) as:

$$y(x,t) = \sum_{n=1}^{\infty} b_n\cos\left(\frac{wt - \gamma_n}{2}\right)\sin(n\pi x), \tag{4.22}$$

where b_n and γ_n are determined by Eqs. (4.20) and (4.21) for the transient solutions.

For non-trivial ($b_n \neq 0$) steady-state solutions, $D_1 b_n = 0$ and $D_1 \gamma_n = 0$, which yields either $\gamma_n = \frac{\pi}{2}$ or $\gamma_n = \frac{3\pi}{2}$ from Eq. (4.20). Then, from Eq. (4.21), we obtain: $\sigma = \mp \frac{a_1^2}{2\omega_n}$. The fluctuation frequency-amplitude is given from Eq. (4.9) as:

$$w = 2\omega_n \mp \varepsilon \frac{a_1^2}{2\omega_n}. \tag{4.23}$$

A sample plot of Eq. (4.23) is presented in Fig. 4.

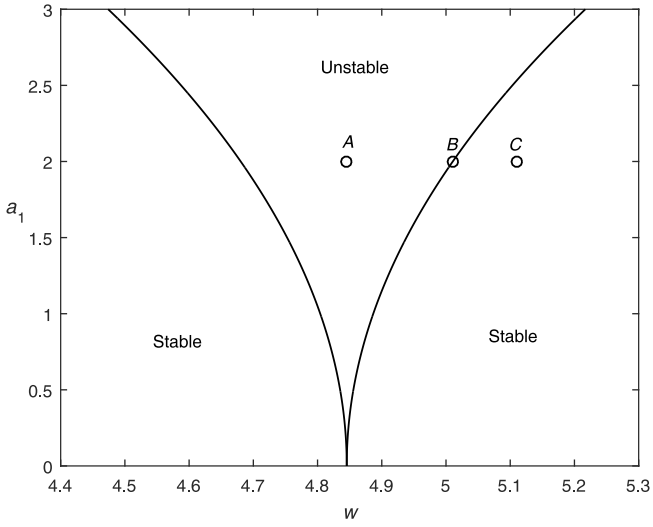

FIG. 4. Fluctuation frequency versus fluctuation amplitudes ($n = 1$, $\omega_1 = 2.4227$, $\varepsilon = 0.2$).

The steady-state bounded solutions occur precisely along the curves. Between the curves, the system is unstable, with solutions growing over time. In the remaining regions of the space, the system is stable.

4.2. Numerical solutions

Equation (4.6) is numerically solved subject to the conditions (4.8). The initial deflection function is chosen as $f(x) = 0.2x(1-x)$. Three different cases, which are indicated as points A, B, and C in Fig. 4 are treated. Point A is in the unstable region, point B is on the stability border, and point C is in the stable region. Plots of the generalized coordinates are given in Figs. 5–7 for the first mode of vibration.

As predicted by the theoretical results, numerical results show that point A is unstable while points B and C are stable.

To numerically construct a stability chart similar to the one shown in Fig. 4, extensive computations are required for each point in the $(w - a_1)$ space. This

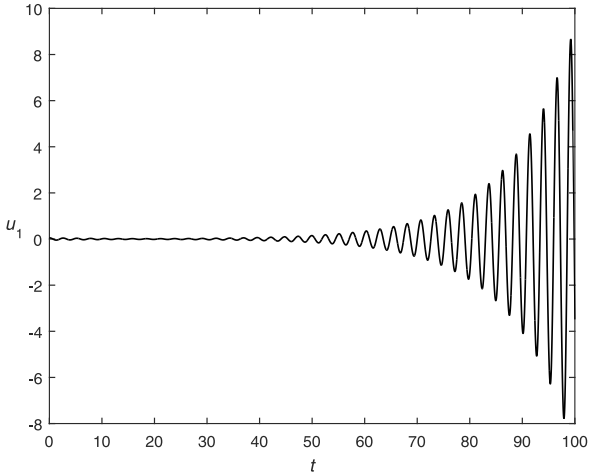

FIG. 5. Time history of point A ($\omega_1 = 2.4227$, $\varepsilon = 0.2$, $w = 4.8454$, $a_1 = 2$).

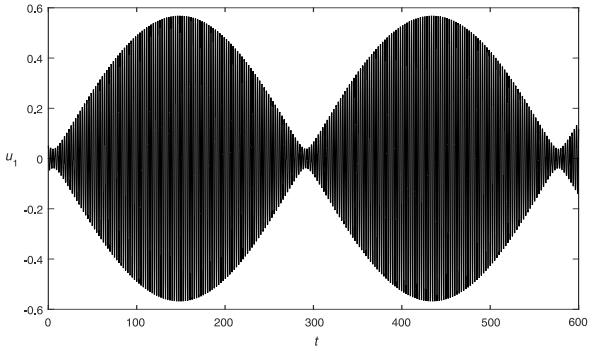

FIG. 6. Time history of point B ($\omega_1 = 2.4227$, $\varepsilon = 0.2$, $w = 5.0105$, $a_1 = 2$).

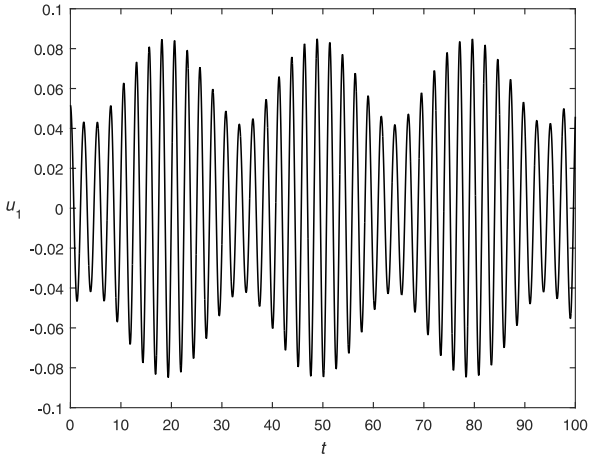

FIG. 7. Time history of point C ($\omega_1 = 2.4227$, $\varepsilon = 0.2$, $w = 5.1105$, $a_1 = 2$).

requires integrating the differential equation for one period, calculating the monodromy matrix, and then determining its eigenvalues, which govern the stability. High resolution is needed for this task to determine the exact locations of the stability boundaries. Perturbation methods have proven effective in determining such stability boundaries with acceptable agreement with the numerical solutions. For small torsional vibrations of rotating blades, the match is almost perfect [19]. The advantage of the theoretical analysis is that the stability boundaries can be calculated analytically. However, this approach has the disadvantage of small discrepancies at lower fluctuation amplitudes, with these discrepancies growing for higher amplitudes. In contrast, while the precise locations of the stability boundaries can be computed numerically, this task requires extensive computation resources.

4.3. Stability analysis via the Mathieu equation

Equation (4.5) can be modified such that the harmonic variations are expressed in terms of a cosine function:

$$\frac{\partial^2 y}{\partial x^2} + \left(a_0^2 + \varepsilon a_1^2 \cos(wt)\right) y = \frac{\partial^2 y}{\partial t^2}. \tag{4.24}$$

Assuming the same solution form as given in Eq. (3.1), the generalized coordinates are expressed as:

$$\ddot{u}_n + \left(\omega_n^2 - \varepsilon a_1^2 \cos(wt)\right) u_n = 0. \tag{4.25}$$

Next, we perform the time transformation:

$$\tau = \frac{w}{2} t, \tag{4.26}$$

which yields:

$$\frac{w^2}{4} u_n'' + \left(\omega_n^2 - \varepsilon a_1^2 \cos(2\tau)\right) u_n = 0, \tag{4.27}$$

where the prime denotes differentiation with respect to the new time variable. Reorganizing Eq. (4.27), we obtain:

$$u_n'' + (\delta + 2\epsilon \cos(2\tau)) u_n = 0, \tag{4.28}$$

which is the standard Mathieu equation with the new parameters defined as:

$$\delta = \frac{4\omega_n^2}{w^2}, \qquad \epsilon = -\varepsilon \frac{2a_1^2}{w^2}. \tag{4.29}$$

Stability diagrams in $\delta - \epsilon$ space can then be used from the literature. See [13] for a sample stability diagram.

5. Concluding remarks

The problem of a rotating string-mass hanged from top was investigated. Both constant rotation speeds and variable rotations about a mean speed were considered. For the constant rotation case, exact analytical solution was given. For the variable rotation case, principle parametric resonances were analyzed. Using the method of multiple scales, the boundaries separating stable and unstable regions were calculated analytically. Numerical integrations of the differential equation confirmed the qualitative behavior predicted by the theoretical analysis.

Developing nonlinear mathematical models for the problem is a potential area for further research. When the total mass of the string is the same order as the attached mass, the tension force becomes variable, leading to an improved mathematical model. More precise stability charts can be developed by considering higher-order perturbations, or by conducting extensive numerical calculations. Additionally, other resonance types may be considered in the context of nonlinear models.

Competing interests

The author declares no competing interests.

References

1. Pakdemirli M., Mathematical modelling of hanging rope problem subject to rotation, *International Journal of Mathematical Education in Science and Technology*, 2024, https://doi.org/10.1080/0020739X.2024.2352424.

2. Triantafyllou M.S., Triantafyllou G.S., The paradox of the hanging string: an explanation using singular perturbations, *Journal of Sound and Vibration*, **148**(2): 343–351, 1991, https://doi.org/10.1016/0022-460X(91)90581-4.

3. Lin B., Ravi-Chandar K., An experimental investigation of the motion of flexible strings: Whirling, *ASME Journal of Applied Mechanics*, **73**(5): 842–851, 2006, https://doi.org/10.1115/1.2172270.

4. Coomer J., Lazarus M., Tucker R.W., Kershaw D., Tegman A., A non-linear eigenvalue problem associated with inextensible whirling strings, *Journal of Sound and Vibration*, **239**(5): 969–982, 2001, https://doi.org/10.1006/jsvi.2000.3190.

5. Belmonte A., Shelley M.J., Eldakar S.T., Wiggins C.H., Dynamic patterns and self-knotting of a driven hanging chain, *Physical Review Letters*, **87**(11): 114301, 2001, https://doi.org/10.1103/PhysRevLett.87.114301.

6. Temnenko V.A., Bifurcation of the shape of a rotating string, *Journal of Mathematical Sciences*, **82**(2): 3347–3350, 1996, https://doi.org/10.1007/BF02363999.

7. Wang C.Y., Wang C.M., Freund R., Vibration of heavy string tethered to mass–spring system, *International Journal of Structural Stability and Dynamics*, **17**(4): 1771002, 2017, https://doi.org/10.1142/S021945541771002X.

8. Deschaine J.S., Suits B.H., The hanging cord with a real tip mass, *European Journal of Physics*, **29**(6): 1211–1222, 2008, https://doi.org/10.1088/0143-0807/29/6/010.

9. Wang C.Y., Stability of an axially rotating heavy chain with an end mass, *Acta Mechanica*, **46**(1): 281–284, 1983, https://doi.org/10.1007/BF01176779.

10. Wang C.Y., Wang C.M., Exact solutions for vibration of a vertical heavy string with a tip mass, *The IES Journal Part A: Civil & Structural Engineering*, **3**(4): 278–281, 2010, https://doi.org/10.1080/19373260.2010.521623.

11. Wang C.Y., Stability and large displacements of a heavy rotating linked chain with an end mass, *Acta Mechanica*, **107**(1–4): 205–214, 1994, https://doi.org/10.1007/BF01201830.

12. Noël J.M., Niquette C., Lockridge S., Gauthier N., Natural configurations and normal frequencies of a vertically suspended, spinning, loaded cable with both extremities pinned, *European Journal of Physics*, **29**(5): N47, 2008, https://doi.org/10.1088/0143-0807/29/5/N02.

13. Nayfeh A.H., *Introduction to Perturbation Techniques*, John Wiley and Sons, New York, 1981.

14. Nayfeh A.H., Mook D.T., *Nonlinear Oscillations*, John Wiley & Sons, New York, 2008.

15. Pakdemirli M., Understanding the physics of eigenvalue-eigenfunction problems: Rotating beam problem, *International Journal of Mechanical Engineering Education*, 2024, https://doi.org/10.1177/03064190241261512.

16. Pakdemirli M., Vibrations of a vertical beam rotating with variable angular velocity, *Partial Differential Equations in Applied Mathematics*, **12**: 100929, 2024, https://doi.org/10.1016/j.padiff.2024.100929.

17. Pakdemirli M., Complex exponential method for solving partial differential equations, *Engineering Transactions*, **72**(4): 461–474, 2024, https://doi.org/10.24423/EngTrans.3334.2024.

18. Pakdemirli M., Strategies for treating equations with multiple perturbation parameters, *Mathematics in Engineering, Science and Aerospace MESA*, **14**(4): 1–18, 2023.

19. Al-Nassar Y.N., Kalyon M., Pakdemirli M., Al-Bedoor B.O., Stability analysis of rotating blade vibration due to torsional excitation, *Journal of Vibration and Control*, **13**(9–10): 1379–1391, 2007, https://doi.org/10.1177/1077546307077454.

Received December 1, 2024; accepted version January 22, 2025.
Online first March 4, 2025.